

Coping with failed elements on an array: a modelling approach to the technical justification

C Nageswaran

Submitted 17.01.10
Accepted 03.06.10

Ultrasonic inspections using array probes programmed to manipulate the field to focus and steer the sound energy are now widely applied in key industries to ensure the integrity of expensive and critical components or structures. These phased array probes are often fragile when used in field inspections and the failure of elements on the array can be an expensive affair, not just in terms of financial cost but also the implications towards the integrity of the inspection. This paper provides a technical justification for dealing with failed elements and aims to establish the tolerable limits through the use of modelling.

Keywords: phased array, ultrasonic, failed elements, technical justification, modelling.

1. Introduction

This paper discusses the use of the CIVA⁽¹⁾ simulation package, developed by the Commissariat de l'Energie Atomique (CEA) of France, to study the effect of failed elements in a linear array when generating ultrasonic beams. Both CIVA and the SimulUS⁽²⁾ software (developed by Peak NDT, Derby) have previously been shown to be capable of modelling the changes in sound field characteristics due to the failure of elements^(3,4). In this study, towards developing evidence for a generic phased array technical justification, modelling was used to evaluate the tolerable number of elements that could be lost.

Element failure often occurs due to physical damage to the cable, wear plate and connecting pins. The failure of elements can give rise to strong sound pressure in regions which lie off the main sound beam path (axis). If such artefacts are sufficiently strong, they can give rise to spurious echoes during inspection. At best these echoes would complicate the interpretation and positioning of flaws; at worst they can lead to the false sizing of flaws. Hence, it is important to provide guidance, in any ultrasonic procedure for inspection using phased array probes, as to how many failed elements can be accepted.

2. Approach

2.1 Cases

Two inspection scenarios (one with the array focusing and the other with it steering) were modelled to study the effect of failed elements on the integrity of the ultrasonic beam. The following four beam parameters were measured from the model outputs:

1. 6 dB beam width (measured perpendicular to the beam axis).
2. Strength of artefacts (side lobes and grating lobes).
3. Beam angle.
4. Absolute beam strength.

Two cases of phased array beams, generated by two linear arrays, were considered:

- Case A – 45° beam focused at 75 mm depth; beam is not electronically steered. The probe aperture is composed of 32 elements generating sound at 5 MHz;
- Case B – 60° beam generated by electronic steering; the beam is not focused. The probe aperture is composed of 16 elements, generating sound at 2 MHz.

Furthermore, in both cases above, two types of element failure were studied:

- Type 1 – Random failure of elements;
- Type 2 – Failure of a block of contiguous elements along different regions of the array.

In type 1 failure, increasing numbers of elements were switched off in the model to simulate their complete failure. These elements were randomly chosen on the array but prevented from being adjacent to each other.

In type 2 failure, a number of adjacent elements were made inactive within a contiguous group of elements. This contiguous group was placed at the bottom of the array (Figure 1(a)), centrally aligned in the middle of the array (Figure 1(b)) and top of the array (Figure 1(c)).

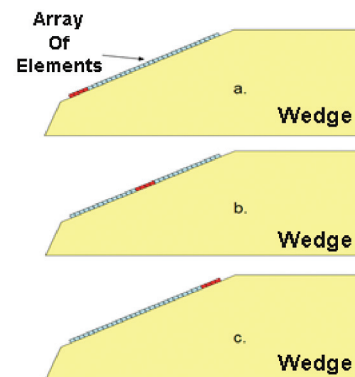


Figure 1. Failed element modelling of the type 2 cases: a contiguous group of failed elements at the bottom of the array (a), centrally on the array (b) and at the top (c)

An element was made inactive by reducing its amplitude of displacement to zero. Hence, the focal laws were calculated for the entire set of elements in the array; then the elements to be made inactive were not 'fired' when the sound field was created.

2.2 Parameters

Table 1 is a summary of the probe, wedge, component and ultrasonic parameters used in the study. PW refers to a pulse wave input waveform of about 2.5 cycles containing a range of frequencies with a central frequency of 5 MHz (case A) and 2 MHz (case B). The models for case A type 1 were run with continuous wave (CW) input waveforms and those in case A type 2 were run with pulse wave input waveforms. Previous experience⁽²⁾ showed that CW

Channa Nageswaran is with TWI Ltd, Granta Park, Great Abington, Cambridge CB21 6AL, UK. Tel: 01223 899000; Email: channa.nageswaran@twi.co.uk

models are more pessimistic in comparison to PW models.

Note that in case B, without electronic steering, the array will produce a shear wave beam at 45° in the ferritic steel component due to the wedge angle being set at 30.7°. The crossbeams for case B were generated in the far field of the probe where the CIVA model was previously validated⁽²⁾.

Table 1. Probe, wedge and component parameters used in the present investigation

Case	A (Focusing)	B (Steering)
Probe frequency	5 MHz	2 MHz
Elements in active aperture (A)	32	16
Element pitch (p)	1.2 mm	1.6 mm
Element width (e)	0.9 mm	1.5 mm
Inter-element gap (g)	0.3 mm	0.1 mm
Passive aperture (W)	12 mm	15 mm
Wedge longitudinal velocity	2330 m/s	2330 m/s
Wedge angle	30.7°	30.7°
Beam type	Shear	Shear
Material type	Ferritic steel	Ferritic steel
Material longitudinal velocity	5894 m/s	5894 m/s
Material shear velocity	3206 m/s	3206 m/s
Signal type (pulse width)	PW (1.193 μs) & CW	PW (1.278 μs)
Focal depth or calculation depth	75 mm	75 mm
Beam angles	45°	60°

2.3 Terms of reference

Figure 2 shows the linear array composed of two primary axes: the passive axis and the active axis. The elements lie adjacent to each other along the active axis and phasing is only possible along the active axis. Along the passive axis the sound pressure field behaves according to physical laws applicable to a fixed size radiator. In the array of Figure 2 there are a total of 16 elements (as in case B) but only the set of red elements are functional; the yellow elements are in the active group but are ‘down’ and hence do not generate sound – these are considered to be random failed elements (type 1).

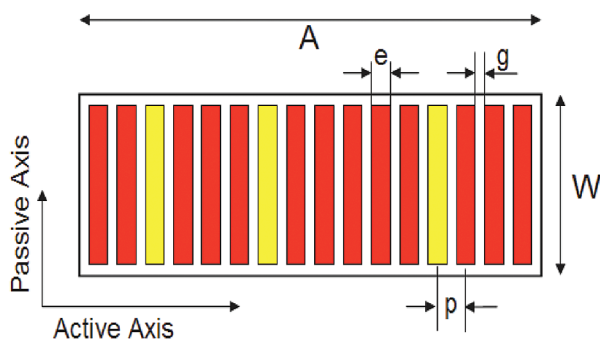


Figure 2. Representation of a linear array and its primary axes, along with the definition of element width (e), gap (g), pitch (p), passive aperture (W) and active aperture (A); the yellow elements are ‘failed’

Figure 3 shows the inspection scenario with the linear array probe, wedge and component for case A (45° shear wave beam in ferritic steel). From the model outputs the four beam parameters (see Section 2.1) were evaluated.

The model output shown in the control volume of Figure 3 is the sound pressure along the axis of the beam. Using this output and the 6 dB field depth of the sound about its focal point, changes

in the beam angle due to failed elements can be evaluated. This method of beam angle evaluation based on the field is only possible in case A where the sound is focused leading to a sufficiently small field depth.

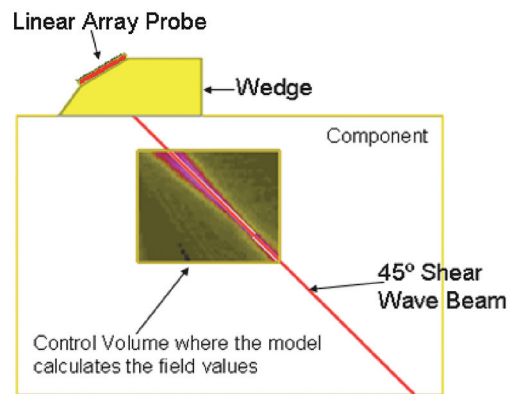


Figure 3. Representation of the linear array on its wedge propagating a 45° shear wave beam into the ferritic steel component

Figure 4 shows the crossbeam at the focal depth of 75 mm for case A. The model output generates a two-dimensional map of the sound pressure and the pressure variation along the line XX (active axis) can be extracted. It is then possible to evaluate the 6 dB beam widths (along the active and passive axes).

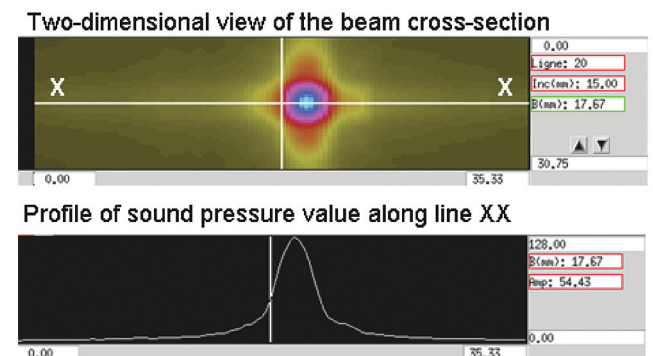


Figure 4. The crossbeam at the focal depth of 75 mm (case A) along with the cross-section pressure profile plotted along line XX through the beam

In the present study, data was collected in two types of control volumes:

- A control volume in the plane of the active axis of the linear array in order to measure the beam angle (as shown in Figure 3);
- A control volume perpendicular to the main beam axis – 75 mm depth in both cases (as shown in the three-dimensional representation in Figure 5).

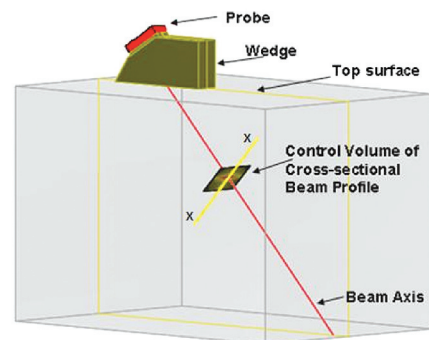


Figure 5. The control volume is perpendicular to the beam axis to measure the cross-section profile of the sound beam at a depth of 75 mm

The cross-section profiles (as in Figure 4) were used to evaluate the beam widths along the active and passive axes. The absolute value of the peak sound pressure of the beam is output by the model; this quantity is proportional to the unit of sound pressure and can be used to evaluate the effect on the absolute strength of the beam due to failed elements.

In pulse echo inspection, the primary concern is the strength of any spurious echoes which return to the probe. Hence, the sound pressure output of the CIVA model, which gives the elastodynamic quantity at the evaluation point (control volume), is converted to the equivalent strength of the signal which would be expected at the probe had an echo been generated at the control volume region. In essence, the signal strength that would be recorded by the pulse echo probe is proportional to the square of the sound pressure at the reflector.

2.4 Acceptance criteria

The threshold criterion is based on the strength of beam artefacts due to element failure. An 'artefact' is defined as any feature of the sound beam away from the main beam axis, which includes side energy lobes and grating lobes generated by array probes⁽⁵⁾. Provided that the pulse echo signal strength from a point reflector due to the beam artefact is equal to or greater than 20 dB below the peak signal strength of the main beam, the integrity of the sound field generated by the phased array probe is considered acceptable.

The threshold value of 20 dB has been chosen as it represents an ultrasonically acceptable difference between an echo of significance and those which are considered to be spurious. In practice, the echo generated by a reflector (flaw or discontinuity) due to the main sound beam could be saturated (that is greater than 100% screen height on the detecting instrument). The signal returned by the same reflector due to the artefacts in the beam could then be significant. The present criterion assumes that the inspection is appropriately calibrated to ensure that echoes from the expected flaw targets will remain below the amplitude level which can be recorded as a finite value by the ultrasonic instrument.

Figure 6 shows the cross-section profile along the active axis of the received signal in pulse echo with six failed elements (in an active aperture of 16) in type 2(b) mode (contiguous set at centre

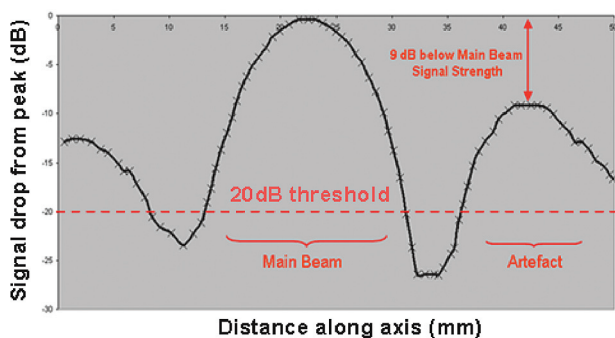


Figure 6. Example of the cross-section profile along the active axis for an array with six failed elements. The pulse echo signal strength due to the artefact is 9 dB below that from the main beam

of array). The field strength along the beam axis has its peak signal at 0 dB. There is a strong artefact adjacent to the beam which is 9 dB weaker than the main beam. Following the stated criterion, six random failed elements (out of 16) is not acceptable because the received signal from a reflector due to the artefact can seriously affect interpretation, positioning and sizing.

3. Results and discussion

The results are presented as a discussion of the two types of element failure: random (type 1) and contiguous groups (type 2).

3.1 Random element failure (type 1)

Random element failure models were generated in cases A and B, but the severity of the random failure was simulated in two different ways. In both cases, increasing failed elements represented increasing severity. However, in case A the failed elements in each model run were different and in case B the failed elements were the same as in the previous model but for an increment of one. This is summarised in Table 2.

Figure 7 is a summary of the cross-section profiles through the active axis for case A (32 elements in the aperture) showing the relative sound pressure amplitudes. The curves in Figure 7 were plotted along the XX line as illustrated in Figure 4. Figure 7 shows the data as a change from the peak signal strength (of each data set) expressed in dB. The analysis of the data is summarised in Table 3.

Table 2. Random failed element numbers in cases A and B

Number of failed elements	Case A failed element numbers	Case B failed element numbers
2	12, 21	
3		3, 9, 7
4	1, 5, 11, 19	3, 9, 7, 5
5		3, 9, 7, 5, 13
6	3, 9, 13, 16, 18, 22	
9	8, 5, 10, 13, 17, 20, 24, 25, 29	

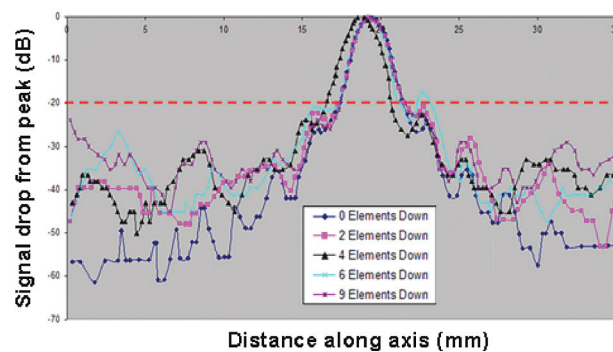


Figure 7. The amplitude cross-section profiles along the active axis for increasing number of failed elements of type 1 failure in case A, expressed as a dB signal strength loss relative to the peak signal strength

Table 3. Summary of analysis in case A type 1 element failure models

No of failed elements	Active axis 6 dB beam width, mm	Passive axis 6 dB beam width, mm	Max artefact signal level (relative to main beam) active axis	Measured beam angle, °	Input wave type	Beam strength loss at focal point, dB
0	3.07	9	24	44.5	CW	0.00
2	2.85	9	21.6	43.5	CW	0.58
4	3.06	9	23.6	45	CW	1.30
6	2.84	9	18	45.2	CW	1.89
9	2.92	9	24.8		CW	2.63

The effect on the active axis beam width is a reduction in the measured width; the maximum reduction is evaluated to be 7.5% when six elements have failed. However, there does not appear to be a pattern between change in beam width and the number of randomly failed elements, given the limited number of random failure cases modelled in this study. Hence, to evaluate the actual change in beam width due to a given set of failed elements, that particular case must be modelled.

As expected, the passive axis beam width does not vary with failing elements, which is consistent with the physical laws governing the propagation of the elastodynamic sound from a fixed size radiator.

There appears to be a change in the beam angle as the elements fail. However, it is within the error of 1.5° due to the resolution of the models and the method used to calculate the beam angle. Increasing numbers of failed elements will have an effect on the beam angle as the index point is influenced (see Section 3.3).

Note also that this data set is computed using a CW input – *ie* the frequency content of the input waveform is constant at 5 MHz. This is known to induce the creation of strong side energy lobes in the model outputs in comparison to a PW input where there is a range of frequencies in the waveform⁽²⁾. Hence, the strength of the artefacts (such as side lobes) generated subsequently give a pessimistic view. Table 3 shows that when six elements are defective the strength of the pulse echo side lobe is 18 dB below the peak of the main beam. This implies that the beam is not acceptable for inspection based on our criterion. However, it is not possible to put a threshold value for acceptable element failure at six, since when nine elements are defective the strength of the artefact is acceptably 24.8 dB below peak. It appears that the nature of random element failure makes it difficult to provide guidance based on trends. A further model was run with a PW input waveform, which is closer to reality, and three failed elements. In that case the strength of the artefact was 23.8 dB below peak. It suggests that, based on the available evidence for a random type failure in case A, the inspection procedure should allow a maximum of three elements to fail.

The CIVA model is able to evaluate the relative loss in the maximum sound pressure (at the focal point) as an increasing number of elements become defective. This is summarised in the last column of Table 3. As one would expect, as the number of failed elements increases, the maximum sound pressure values decrease, leading to a maximum loss of 2.68 dB when nine elements are defective.

An interesting feature that can be seen in Figure 7 is a shift in the position of the peak signal when four elements are defective, whereas the other curves representing element failure lie close to the case when no elements have failed. The shift in the peak signal in the ‘4 Elements Down’ case is less than 1 mm. The reason is likely to be due to the nature of the failed element distribution on the array (see Table 2) in that they are biased towards one side of the array.

Table 4 is a summary of the analysis of type 1 models run in case B. In case B the array contains half the number of elements (16) as opposed to case A (32) and the frequency of the probe in case B is lower at 2 MHz as opposed to 5 MHz in case A. Furthermore, cases A and B independently model the two major capabilities achievable by ‘phasing’ the array: focusing and steering, respectively.

All the models in case B type 1 failure were run with PW input

waveforms. Also, it was not possible to evaluate the beam angle as the control volume was not large enough to encompass the 6 dB field depth. Since the sound is not focused in case B, the size of the field depth is large in comparison to case A and the reasons for limiting this study are discussed in Section 3.3.

Note that the beam widths (along both the active and passive axes) are significantly larger in comparison to case A. Unlike the type 1 failures of case A, as the number of failed elements increases, the element number along the array is kept constant (see Table 2). As the number of failed elements increases to five elements, the active axis beam width reduces by 7.5%. More significant is the increase in the strength of artefacts, which is only 15.4 dB from the peak value when four elements have failed, making the beam unacceptable with regard to the working criterion.

As before, the loss in beam strength is consistent with increasing numbers of failed elements. Figure 8 shows the cross-section profiles for the cases in Table 4, measuring the change in signal strength to each data set’s peak value (expressed in dB).

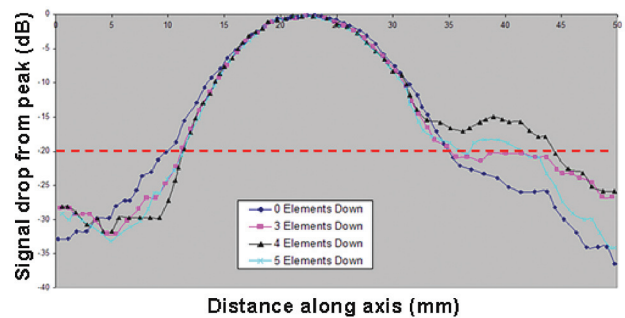


Figure 8. The amplitude cross-section profiles along the active axis for increasing number of failed elements of type 1 failure in case B expressed as a dB signal strength loss relative to the peak signal strength

The failure of three elements leads to the beam being unacceptable according to the criterion – 19.8 dB artefact strength. This implies that the allowable number of failed elements depends on the geometric condition of the particular array. Three failed elements in case A represents a loss of 9.4% of the full sound radiating surface, whereas three failed elements in case B represents 18.8% of the radiating surface. Hence, it may be necessary to approach the acceptable element failure criterion by considering how each failed element affects the total radiating surface. This would then imply that the acceptable number of failed elements depends on other parameters of the linear array: pitch and number of elements in the active aperture. In turn, the dependence on pitch also implies a dependence on the frequency of the probe.

3.2 Contiguous element failure (type 2)

As shown in Figure 1, within the type 2 failure mode the set of contiguous (adjacent) failed elements can be at the bottom (referred to as type 2(a)), about the centre line of the array (referred to as type 2(b)) and at the top of the array (referred to as type 2(c)). In the study, models were run in the type 2(a) and type 2(b) configurations only. It is noted, through logical reasoning, that configuration types 2(a) and 2(c) would have the same effect of rotating the field about the main axis of the beam (represented by the index point and beam angle).

Table 4. Summary of analysis in case B type 1 element failure models

No of failed elements	Active axis 6 dB beam width, mm	Passive axis 6 dB beam width, mm	Max artefact signal level (relative to main beam) active axis	Measured beam angle, °	Input wave type	Beam strength loss at focal point, dB
0	19.34	22	26.4		PW	0.00
3	18.09	22	19.8		PW	1.92
4	18.09	22	15.4		PW	2.73
5	17.89	22	18.2		PW	3.47

Table 5 shows the summary of the analysis of case A type 2 models. As expected, the passive axis beam width is not affected by element failure. In configuration type 2(a), the maximum variation of the active axis beam width is 21.2%. The active axis beam width increases as the number of failed elements increases. This is consistent with the physical laws governing ultrasound generation from a finite size radiator where the divergence of the beam is inversely proportional to the size of the radiator: as the aperture of the radiator is reduced (as in configuration type 2(a)) the divergence of the sound field is increased in the far field, leading to a larger beam size at a given point.

When a maximum of five elements have failed in configuration type 2(a), the loss in absolute signal strength is 1.64 dB. The change in the beam angle is within the accuracy of the evaluation method (1.5°) – see Section 3.3. The largest effect on the strength of artefacts is only 1.6 dB when four elements are down, as illustrated in Figure 9.

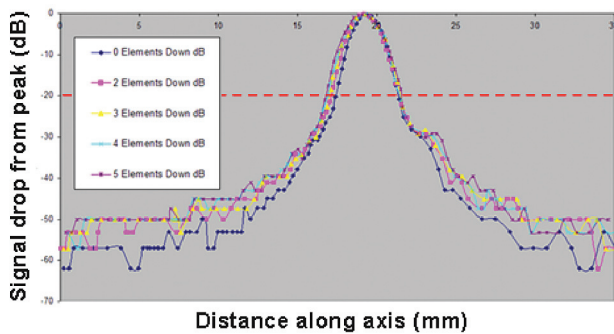


Figure 9. The amplitude cross-section profiles along the active axis for increasing number of failed elements of type 2(a) failure in case A, expressed as a dB signal strength loss relative to the peak signal strength

When five elements have failed in configuration type 2(a), the effective aperture has been reduced along the active axis direction. This leads to an increase in the divergence of the beam in the far field and a widening of the beam width along the active axis. However, the differences in the beam profiles only become significant well outside the 6 dB beam width of the main beam. Based on this evidence, the stated criterion for the allowable number of failed elements is satisfied in all the models: even after five elements have failed, the generated beam is still acceptable.

Hence, with the available evidence, the number of acceptable failed elements is greater than five when they fail in the type 2(a) configuration. Furthermore, unlike in the type 1 failure, the beam profile is a lot cleaner in the type 2(a) configuration, lacking strong artefacts along the active axis direction.

Configuration type 2(b) models (as summarised in Table 5 for

case A) show different behaviour to configuration type 2(a). As the number of failed elements increases, the active axis beam width reduces steadily. When eight elements have failed (four either side of the centre line of the array), the active axis beam width is reduced by 12.3%. The increase in the strength of the artefacts is more dramatic: when eight elements are down, the strongest artefact is only 14 dB weaker than the main beam, failing the acceptance criterion. Figure 10 shows the cross-section profiles for case A type 2(b). Figure 11 shows the crossbeams, which is the same data given in Figure 10 but in a two-dimensional representation where signal strengths are plotted using a colour scale, as shown in Figures 4 and 5.

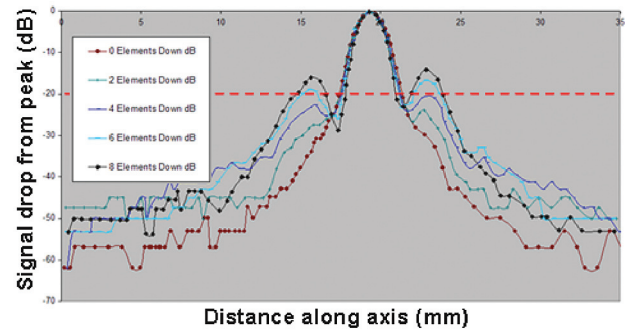


Figure 10. The amplitude cross-section profiles along the active axis for increasing number of failed elements of type 2(b) failure in case A, expressed as a dB signal strength loss relative to the peak signal strength

The artefacts in configuration type 2(b) are due to diffraction effects (known as grating lobes). Strong sound pressure regions either side of the main beam are due to constructive interference of sound pressure emanating from essentially two sources equally spaced either side of the centre line of the array; the effect due to failed elements at the centre of the array is to divide the array into two separate radiating entities. The artefacts either side of the main beam would be symmetrical had the array not been propagating sound at an angle within the component. As the strength of the beam is dependent on the angle of refraction within the component, the artefact on one side of the main beam (lower refraction angle) is stronger than on the other side (higher refraction angle); this is illustrated two-dimensionally in Figure 11.

With the evidence available, the acceptable number of elements that can fail is four, based on the 20 dB threshold for artefact strengths (see Table 5). Figure 15 shows that, as in configuration type 2(a), in configuration type 2(b) failure the position of the beam within the component at the focal point does not appear to be altered. The change in beam angle also remains within the error of the method used for its evaluation.

Table 5. Summary of analysis in case A type 2 element failure models

No of failed elements	Position	Active axis 6 dB beam width, mm	Passive axis 6 dB beam width, mm	Max artefact signal level (relative to main beam) active axis	Measured beam angle, °	Input wave type	Beam strength loss at focal point, dB
0		3.07	9	29.6		PW	0.00
2	A	3.21	9	29.8	46.3	PW	0.54
3	A	3.43	9	29	45.2	PW	0.91
4	A	3.5	9	31.2	45.7	PW	1.21
5	A	3.72	9	29.2	45.2	PW	1.64
2	B	2.92	9	24.8	45	PW	0.53
4	B	2.77	9	20.2	45	PW	1.11
6	B	2.63	9	16.6	44.8	PW	1.73
8	B	2.56	9	14	44.4	PW	2.41

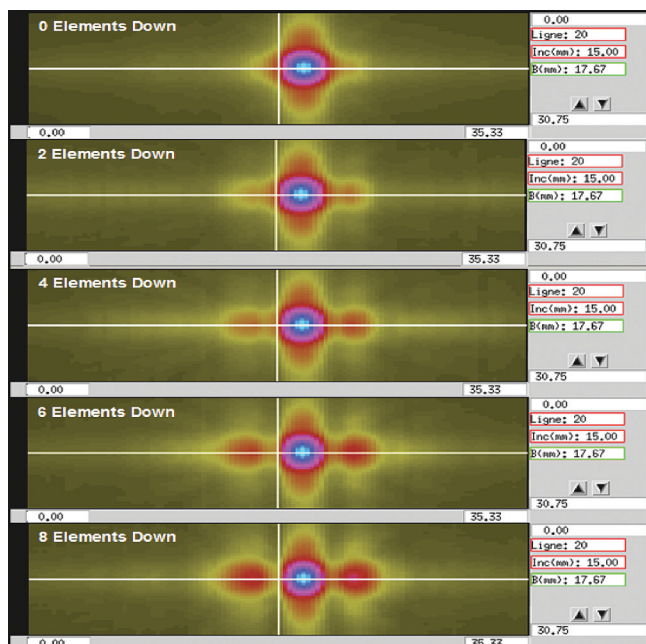


Figure 11. Two-dimensional representations of the crossbeams due to failed elements. The area represented is 35.33 mm (horizontally) by 30.75 mm (vertically), and maximum signal strength is represented by bright blue. Case A, type 2(b)

Table 6 shows the summary of the analysis of case B type 2 element failure models. Note that, again, due to limitation on the control volume size it was not possible to evaluate the beam angle using the 6 dB field depth method (see Section 3.3). Another control volume limitation in the available set of data for case B configuration type 2(a) implied that it was not possible to observe any artefacts. The physical differences between cases A and B have been stated previously (Section 3.1).

For case B configuration type 2(a), only model data for the influence of failed elements on the active axis beam width exist (see Table 6). Figure 12 shows the crossbeams of case B configuration type 2(a) for increasing numbers of failed elements. As shown in Table 6, the increase in the beam width when the number of failed elements increases from three to six is 39.4%, which is a greater change than in case A configuration type 2(a) between none and five failed elements (21.2%).

Along with the rapid increase in the beam width along the active axis, note the migration of the main beam centre as the number of failed elements increases; this is attributed to the index point migration. The shift in beam centre position is around 5 mm going from no failed elements to six failed elements.

For case A configuration type 2(a) failure, the shift in the position of the beam was small, in comparison to case B configuration type 2(a). Due to the larger pitch size and the increased wavelengths in

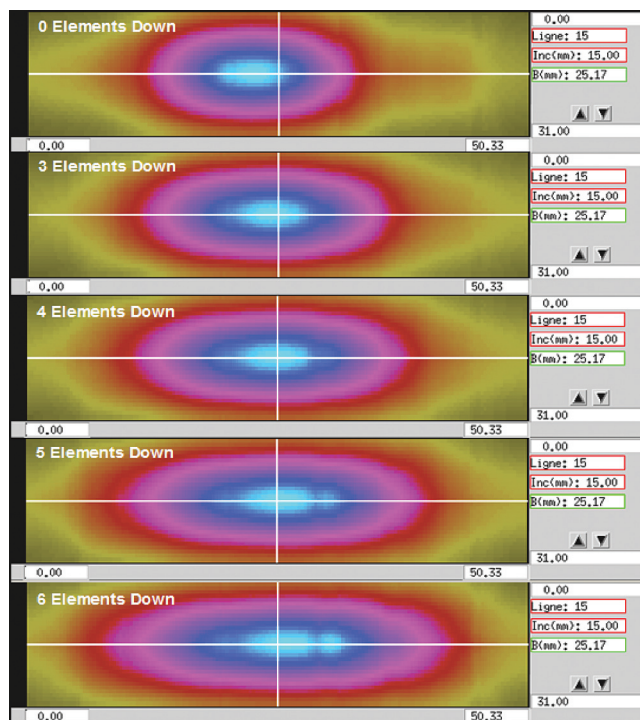


Figure 12. Two-dimensional representations of the crossbeams due to failed elements. The area represented is 50.33 mm (horizontally) by 31 mm (vertically), and maximum signal strength is represented by bright blue. Case B, type 2(a)

case B (as opposed to case A), the effects due to configuration type 2(a) are more pronounced. Furthermore, in case A the focal law was designed to focus the beam whereas in case B the focal law was steering the beam; this implies that the shift in beam position due to configuration type 2(a) failure is dependent on the type of electronic phasing applied to the linear array.

In case B configuration type 2(b), the decrease in active axis beam width when the number of failed elements increases from 2 to 6 is 16.5%. The effects of diffraction are dominant in generating the artefacts; when six elements have failed in configuration type 2(b), the strongest artefact is only 8.6 dB weaker than the main beam (see Table 6). The reason why changes to beam widths and artefact sizes are greater in case B in comparison to case A is geometrical, as discussed in Section 3.1. The actual sound radiating area lost due to a single failed element in case A is 3.1% whereas it is 6.3% in case B.

Along with large gap sizes between the two discrete source points while in configuration type 2(b) due to geometry, the failure of just two elements in case B leads to the beam losing its integrity according to the 20 dB threshold criterion; in case A configuration type 2(b), up to four elements could fail before the probe was deemed unacceptable (see Table 5).

Table 6. Summary of analysis in case B type 2 element failure models

No of failed elements	Position	Active axis 6 dB beam width, mm	Passive axis 6 dB beam width, mm	Max artefact signal level (relative to main beam) active axis	Measured beam angle, °	Input wave type	Beam strength loss at focal point, dB
3	a	22.98	22			PW	0.00
4	a	25.58	22			PW	0.75
5	a	28.08	22			PW	1.58
6	a	32.03	22			PW	2.52
2	b	17.47	22	20.2		PW	0.00
4	b	16.12	22	13.8		PW	0.83
6	b	14.58	22	8.6		PW	2.39

Figure 13 shows the cross-section profiles of case B configuration type 2(b) for increasing numbers of failed elements. Note that in configuration type 2(b) there is no shift in the main beam position. However, as in the models for case A configuration type 2(b), there is a rapid increase in the strength of the main diffraction induced artefacts either side of the main beam. The strength of diffraction artefacts is determined by the ratio of the gap between the source points and the wavelength of the sound, in addition to the degree of refraction required for their plane of existence. Hence, any guidance on specifying the acceptable number of failed elements needs to take into account the gap between the effective source points (due to configuration type 2(b) element failure) and the frequency at which the sound is being radiated by the probe.

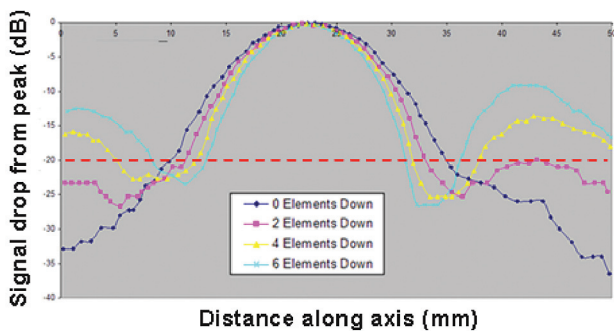


Figure 13. The amplitude cross-section profiles along the active axis for increasing number of failed elements of type 2(b) failure in case B, expressed as a dB signal strength loss relative to the peak signal strength.

In summary, the main effects due to the two configurations of type 2 failure are:

1. Configuration (a): Increase in beam width and shift in position of the main beam centre. The degree of increase in any artefacts depends on geometrical conditions of the array and the frequency of the probe, as well as the number of failed elements in a contiguous group.
2. Configuration (b): The main effects are due to double source diffraction. The beam width is reduced as the number of failed elements increases. There is no shift in the position of the main beam centre but the strength of artefacts increases rapidly with increasing element failure. Again, the severity of artefacts depends on the geometrical conditions of the array and the frequency of the probe.

Furthermore, in configuration type 2(a), the degree of shift in the beam position appears to depend on the type of phasing being applied to the linear array. When the array is being used to steer the sound the shift is greater than when focusing, as suggested by the two cases modelled. However, further work needs to be performed to study this phenomenon using models to observe the beam along the axis. It could be the case that in configuration type 2(a) failure, the beam is being rotated about the focal point and hence shifts in beam position measured using cross-section profiles will become measurable at distances away from the focal point.

3.3 The index point and the beam angle

The index point is defined on the interface between the wedge and the component; it is the geometrical point through which the sound from the finite surface radiator (the linear array) is considered to propagate from one medium to the other. The index point will migrate depending on the size of the radiator (relative to a constant reference point), the wedge angle and the nature of phasing that is done electronically (focusing and/or steering).

In practice, it is not possible to evaluate the index point of a probe as the actual propagation takes place over an area of the wedge/component interface. Similarly, it would be difficult to identify the maximum point of the sound pressure at this interface

without very high resolutions (0.1 mm or less).

Similarly, at the outset of the study, a method was chosen to evaluate the beam angle of the sound in the component. It was to be evaluated using the 6 dB field depth of the beam in the ferritic component. A control volume was placed along the beam axis (as discussed in Section 2.3) to evaluate the beam. It was only possible to perform this cost-effectively for case A (where the sound was focused), as in case B the 6 dB field depths were too large.

Figure 14 shows the beam axis and the definition of the 6 dB field depth of the beam (case A with no failed elements). By plotting the coordinates of points A and B, the beam angle can be evaluated using trigonometry; note that the dimensions of the control volume are 102 mm horizontally and 82 mm vertically.

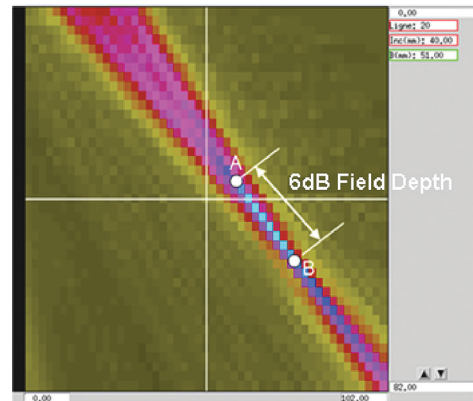


Figure 14. Definition of the 6 dB field depth (case A) is the distance between point A (upstream) and point B (downstream), where field strength is 6 dB below the strength at the focal point (which is in between points A and B)

The resolution of the control volume leads to an inaccuracy in the measured beam angle, which is estimated to be 1.5°. Due to the limited scope of the study, sufficient models were not run to comment conclusively on the effect on beam angles (such as for case B) when elements fail in the array.

Figure 15 shows a set of data for case A type 1 (random) failure. The measured beam angles do not vary from the expected 45° (within the error of the method) but the resolution is not high enough for conclusive evidence. However, it is possible to see the increase in the sound pressure either side of the main beam focus as elements fail. These artefacts can lead to an increase in spurious echoes in pulse echo testing, which could be from defects or be due to the material itself (for example 'grass' noise in coarse-grained materials).

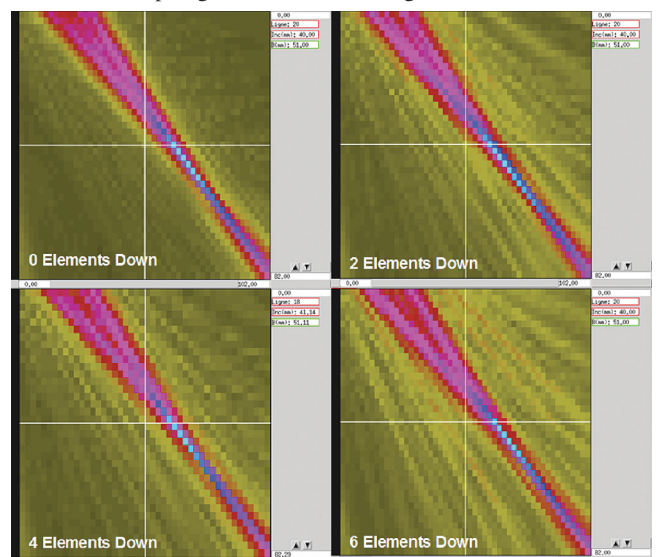


Figure 15. Two-dimensional representations of the beams along axis due to failed elements. The area represented is 102 mm (horizontally) by 82 mm (vertically), and maximum signal strength is represented by bright blue. Case A, type 1

4. Conclusions

Two types of element failure were considered in this paper: random and contiguous groups. The acceptance criterion was based on a threshold value of 20 dB, *ie* the signal strength of artefacts need to be weaker than this threshold with respect to the main beam strength for the beam to be acceptable.

For random type failure (type 1), the failure of around 10% of the elements in the active aperture can be tolerated. Hence, for an array consisting of 16 elements, two elements are allowed to fail. By the same argument, three elements can fail in a random (type 1) mode on a 32-element array.

When contiguous groups of elements fail, their configuration on the array plays an important role in deciding whether the linear array is acceptable for inspection. Furthermore, it appears that the type of phasing that is being performed using the array has an important bearing on the ultrasonic field modifications induced by the failure of contiguous groups of elements:

1. Failure of a contiguous group of elements on the edge of the array (type 2(a)) leads to a general increase in the beam widths which can impact on the resolution of the inspection. Furthermore, there could be a shift in the beam leading to errors in positioning;
2. Failure of a contiguous group of elements at the centre of the array (type 2(b)) leads to the generation of diffraction artefacts. These artefacts can be very strong and the severity depends on the frequency (wavelength) of the sound being generated and the gap between two effective radiating surfaces created by the failed element group.

An important recommendation of the study is that, when the failed elements and their position on the array are known, it is best to simulate the implications on the actual inspection through the use of models such as CIVA and SimulUS.

The study was limited in scope and it was only possible to run and analyse a finite number of models within the time and budget available. Future efforts will consider the impact on inspection integrity due to failure of elements on two-dimensional arrays, where the tolerances may need to be addressed with respect to loss of radiating areas and its distribution, rather than simply as a percentage of overall elements on the array.

This study is also an illustration of how modelling can be used to cost-effectively provide evidence towards technical justifications, when compared to experimental routes.

Acknowledgements

The author would like to acknowledge the guidance, support and reviews provided by Charles Schneider (TWI), Colin Bird (Doosan Babcock) and Robin Shipp (Firecrest Consulting).

References and footnote

1. P Calmon, S Mahaut, S Chatillon and R Raillon, 'CIVA: An expertise platform for simulation and processing NDT data', *Ultrasonics*, Vol 44, pp 975-979, 2006.
2. C Nageswaran, C R A Schneider and C R Bird, 'Sound field modelling using SimulUS', *Insight*, Vol 50, No 5, pp 258-263, May 2008.
3. A C Whittle, 'Preliminary steps to validate a beam model for ultrasonic phased arrays', *Insight*, Vol 48, No 4, pp 221-227, April 2006.
4. R Raillon, M Lozev, R Spencer, E Kerbrat and S Mahaut, 'Application of tandem techniques with mono-elements or phased array probes: simulation and experiments', *Proceedings of the Review of Progress in Quantitative Nondestructive Evaluation*, 2005.
5. R/D Tech, 'Introduction to phased array ultrasonic technology applications', R/D Tech Inc, Canada, ISBN 0-9735933-0-X, 2004.

Copyright © 2010 TWI Ltd.